REPORT DOCUMENTATION PAGE

1. AGENCY USE ONLY (Leave blank)	2. REPORT DATE	3. REPORT TYPE AND DATES COVERED
	13 December 1996	Reprint

4. TITLE AND SUBTITLE
Neutron and Electromagnetic Emissions During the 1990 May 24 Solar Flare

5. FUNDING NUMBERS
PR 2311
TA G4
WU 02

6. AUTHOR(S)

L.G. Kocharov*   G. A. Kovaltsov**   M. A. Shea
Jeongwoo W. Lee*   I. G. Usoskin**   D. F. Smart
H. Zirin*   K. R. Pyle+

7. PERFORMING ORGANIZATION NAME(S) AND ADDRESS(ES)

Phillips Laboratory/GPSG
29 Randolph Road
Hanscom AFB, MA 01731-3010

8. PERFORMING ORGANIZATION REPORT NUMBER

PL-TR-96-2305

9. SPONSORING/MONITORING AGENCY NAME(S) AND ADDRESS(ES)

10. SPONSORING/MONITORING AGENCY REPORT NUMBER

11. SUPPLEMENTARY NOTES

12a. DISTRIBUTION AVAILABILITY STATEMENT

Approved for public release; distribution unlimited

12b. DISTRIBUTION CODE

3. ABSTRACT (Maximum 200 words)

Abstract. In this paper, we are primarily concerned with the solar neutron emission during the 1990 May 24 flare, utilizing the counting rate of the Climax neutron monitor and the time profiles of hard X-rays and γ-rays obtained with the GRANAT satellite (Pelaez et al., 1992; Talon et al., 1993; Terekhov et al., 1993). We compare the derived neutron injection function with macroscopic parameters of the flare region as obtained from the Hα and microwave observations made at the Big Bear Solar Observatory and the Owens Valley Radio Observatory, respectively. Our results are summarized as follows: (1) to explain the neutron monitor counting rate and 57.5–110 MeV and 2.2 MeV γ-ray time profiles, we consider a two-component neutron injection function, $Q(E, t)$, with the form

$$Q(E,t) = N_f \exp[-E/E_f - t/T_f] + N_s \exp[-E/E_s - t/T_s],$$

DTIC QUALITY INSPECTED 4

19961223 031

14. SUBJECT TERMS
Solar flares   Solar-terrestrial physics
Solar particles
Solar neutrons

15. NUMBER OF PAGES

16. PRICE CODE

17. SECURITY CLASSIFICATION OF REPORT	18. SECURITY CLASSIFICATION OF THIS PAGE	19. SECURITY CLASSIFICATION OF ABSTRACT	20. LIMITATION OF ABSTRACT
Unclassified	Unclassified	Unclassified	SAR

NEUTRON AND ELECTROMAGNETIC EMISSIONS DURING THE 1990 MAY 24 SOLAR FLARE

L. G. KOCHAROV,* JEONGWOO W. LEE, and H. ZIRIN

Big Bear Solar Observatory, California Institute of Technology, Pasadena, CA 91125, U.S.A.

G. A. KOVALTSOV and I. G. USOSKIN

A.F. Ioffe Physical-Technical Institute, St. Petersburg 194021, Russia

K. R. PYLE

Laboratory for Astrophysics and Space Research, Enrico Fermi Institute, University of Chicago, Chicago, IL 60637, U.S.A.

and

M. A. SHEA and D. F. SMART

Space Physics Division, Geophysics Directorate, Phillips Laboratory, Hanscom AFB, MA 01731–3010, U.S.A.

Abstract. In this paper, we are primarily concerned with the solar neutron emission during the 1990 May 24 flare, utilizing the counting rate of the Climax neutron monitor and the time profiles of hard X-rays and γ-rays obtained with the GRANAT satellite (Pelaez *et al.*, 1992; Talon *et al.*, 1993; Terekhov *et al.*, 1993). We compare the derived neutron injection function with macroscopic parameters of the flare region as obtained from the Hα and microwave observations made at the Big Bear Solar Observatory and the Owens Valley Radio Observatory, respectively. Our results are summarized as follows: (1) to explain the neutron monitor counting rate and 57.5–110 MeV and 2.2 MeV γ-ray time profiles, we consider a two-component neutron injection function, $Q(E,t)$, with the form

$$Q(E,t) = N_f \exp[-E/E_f - t/T_f] + N_s \exp[-E/E_s - t/T_s],$$

where $N_{f(s)}$, $E_{f(s)}$, and $T_{f(s)}$ denote number, energy, and decay time of the fast (slow) injection component, respectively. By comparing the calculated neutron counting rate with the observations from the Climax neutron monitor we derive the best-fit parameters as $T_f \approx 20$ s, $E_f \approx 310$ MeV, $T_s \approx 260$ s, $E_s \approx 80$ MeV, and $N_f(E > 100\ \text{MeV})/N_s(E > 100\ \text{MeV}) \approx 0.2$. (2) From the H$\alpha$ observations, we find a relatively small loop of length $\approx 2 \times 10^4$ km, which may be regarded as the source for the fast-decaying component of γ-rays (57.5–110 MeV) and for the fast component of neutron emission. From microwave visibility and the microwave total power spectrum we postulate the presence of a rather big loop ($\approx 2 \times 10^5$ km), which we regard as being responsible for the slow-decaying component of the high-energy emission. We show how the neutron and γ-ray emission data can be explained in terms of the macroscopic parameters derived from the Hα and microwave observations. (3) The Hα observations also reveal the presence of a fast mode MHD shock (the Moreton wave) which precedes the microwave peak by 20–30 s and the peak of γ-ray intensity by 40–50 s. From this relative timing and the single-pulsed time profiles of both radiations, we can attribute the whole event as due to a prompt acceleration of both electrons and protons by the shock and subsequent deceleration of the trapped particles while they propagate inside the magnetic loops.

* Visiting Associate from St. Petersburg State Technical University, St. Petersburg, 195251, Russia.

1. Introduction

The 1990 May 24 flare has been observed in many high-energy bands and has thus provided a great deal of information on the high-energy particles (Pyle, Shea, and Smart, 1991; Shea, Smart, and Pyle, 1991; Pelaez *et al.*, 1992; Kocharov *et al.*, 1993; Talon *et al.*, 1993; Debrunner, Lockwood, and Ryan, 1993; Terekhov *et al.*, 1993). In particular the flare was the source of high-energy particle flux detected by the neutron monitor network (Shea, Smart, and Pyle, 1991). The increase in neutron monitor counting rate had two distinct peaks. The characteristics of the second increase (onset time is 21:03 UT) were typical for a solar proton event. The first increase (onset time is 20:49 UT) was of short duration and was detected only by monitors on the day side of the Earth, and the increase in the counting rate was ordered inversely by air mass along the line of sight to the Sun. All these circumstances allowed Shea *et al.* (1991) to ascribe the first increase to the arrival of flare neutrons. The neutron origin of this increase was disputed by Debrunner, Lockwood, and Ryan (1992), but proved correct by Kovaltsov, Efimov, and Kocharov (1993). In a later paper, Debrunner, Lockwood, and Ryan (1993) revised their original conclusion and acknowledged the reality of this solar neutron event. It was realised that an extended emission of neutrons took place at the flare (Kocharov *et al.*, 1993; Debrunner, Lockwood, and Ryan, 1993). However, there was no detailed investigation of possible spectra and time profiles of solar neutrons. Moreover, the data on the 2.2 MeV line, which is produced by neutrons decelerated and captured by protons in the solar atmosphere, were not taken into account.

   In this paper, we investigate the solar neutron injection during the 1990 May 24 flare that best describes the counting rate increase of the Climax neutron monitor and time profiles of γ-ray intensity at 57.5–110 MeV and 2.2 MeV. For this purpose, we assume that the form of the neutron injection function is an exponential decay with time and energy, and derive the *e*-folding energy and time scales by fitting the calculated counting rates with the Climax neutron monitor data under various constraints of the observed time behaviors of the γ-rays. To put our results of parameter fitting on a more realistic physical ground, we compare the results with the source parameters as derived from the optical and microwave observations of this flare which were made at the Big Bear Solar Observatory and the Owens Valley Radio Observatory, respectively. In particular, we pay attention to the fast MHD shock wave (the Moreton wave) as a possible source for the acceleration of particles involved with these radiations. It will be shown that the morphology of the flare active region and the timing of the MHD shock relative to the above-mentioned flare radiation provide essential information relating to the problems of neutron generation and dynamics of protons accelerated during this flare.

   The plan of this paper is as follows: in Section 2, we examine the Hα flare data and the microwave bursts to get the macroscopic parameters of the flare active region. We also describe the observation of the MHD shock emitted from this active region. In Section 3, we make a parameter fit of the neutron injection

function to the observations of the Climax neutron monitor using the γ-ray data from the GRANAT satellite as observational constraints. In Section 4, we show how the derived parameters for neutron injection can be explained, consistent with the Hα and the microwave observations. In Section 5, we discuss our results and the assumption of particle acceleration. A brief summary of the conclusions is given in Section 6.

2. Hα and Microwave Emission

The X9.3 flare on 1990 May 24 occurred at 20:46–21:45 UT in the active region NOAA 6063, located at N33 W78. Earlier a smaller (class M1.3) flare was seen at 19:40–20:03 UT in the same active region. We examine Hα, magnetogram, and white-light pictures of this active region taken at Big Bear Solar Observatory at the times of these two events to determine the source dimension and its structure, which we will make use of in the analysis of the high-energy emission data.

Figures 1(a) and 1(b) show the active region at the Hα center line near the peak times of the M1.3 and X9.3 flares, respectively. In the M1.3 event (Figure 1(a)), a small loop is seen which has a projected height $\approx 8''$ (5.8×10^3 km) and length $\approx 33''$(2.3×10^4 km). In the X9.3 event (Figure 1(b)), which is our primary interest, the Hα brightening is much expanded to a large area ($\approx 140'' \times 25''$), which seems to fully cover the area of active region on magnetogram (Figure 1(c)). We note that Figures 1(a), 1(b), 1(c) are at the same scale. The small loop seen during the M1.3 event (Figure 1(a)) is hardly discernible at the peak of the X9.3 event (Figure 1(b)). However, it manifests itself in the decay phase (after 21:10 UT) as a post loop again, which means that this small loop persists during the course of the two flares.

We also pay attention to the possible presence of a rather big magnetic loop which stands up so high that its presence is not properly manifested in Hα. Evidence for such a possibility is gathered when we look closely at the limb profiles in white-light pictures. Figure 1(d) is an enlarged and over-exposed white-light image where this effect is seen. It is common that the limb is topped with a fog-like layer (denoted by dotted lines parallel to the limb in Figure 1(d)), which is believed to be due to spicules that guide materials to move up from the photosphere along vertical field lines. A hole seen in the limb profiles (indicated by an arrow in Figure 1(d)) can therefore be interpreted as due to the presence of a channel of horizontal magnetic fields that prevents material from moving across the field lines. The width of this hole appears to be $\approx 30''$, which must be only a fraction of the whole circumference of the loop cross section.

More direct information on the presence of such a big loop comes from microwave data. This flare was observed by the Owens Valley Solar Array lying in the east–west direction (Lee, Gary, and Zirin, 1994). The relative visibility (as defined by the ratio of the amplitude from one baseline to the total power) can yield a full width at half maximum (FWHM) of the source brightness under the assump-
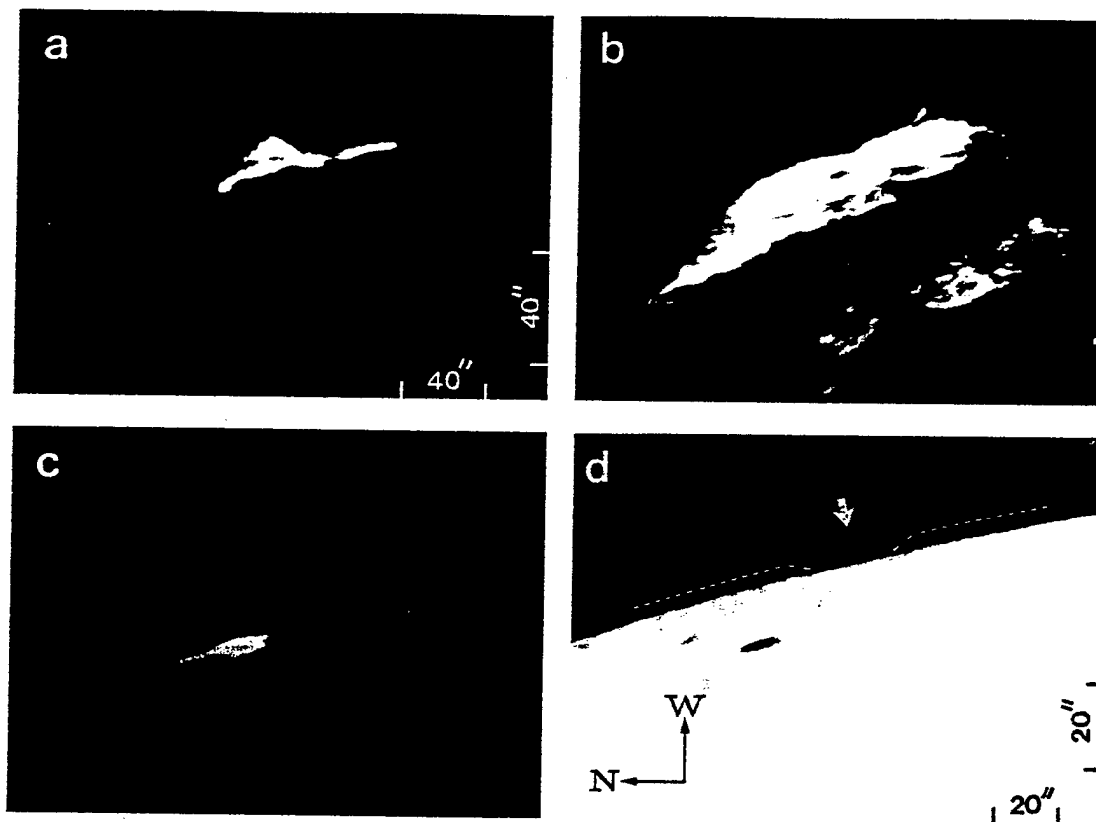
Fig. 1. (a) Hα center line picture of the active region NOAA 6063 at 19:40 UT on 1990 May 24. (b) The same as (a) at 20:49 UT. (c) A magnetogram of the region at 20:50 UT. (d) A white-light picture of the active region showing a hole in the limb profile before the flare. Note that (a), (b), and (c) are in the same scale and (d) is in a different scale as specified.

tion that its distribution takes a gaussian form (Bastian and Gary, 1992). Although a perfect gaussian is not expected for this rather complex source, the FWHM computed in this way gives a scale equivalent to the total area. We show the results in Figure 2; the FWHM of the microwave source comes out as $\approx 200''$ at 1 GHz and decreases rapidly with increasing frequency. The large area ($\approx 200'' \times 200''$) at low frequency (1 GHz) would closely represent the actual projected area of the magnetic structure, since at a frequency as low as 1 GHz, the magnetic loop is likely to be optically thick over most of its volume. The rapid size variation with frequency reflects that the source has nonuniform field distribution in this case.

We note that the size of the microwave source at 1 GHz ($\approx 200'' \times 200''$) is much larger than the size in Hα ($\approx 140'' \times 25''$). Such a large difference between two source sizes may be understandable in terms of the relative location of the two sources and the projection effect on them. The Hα image in this event is reduced in one dimension because the emission comes from the chromosphere and is greatly
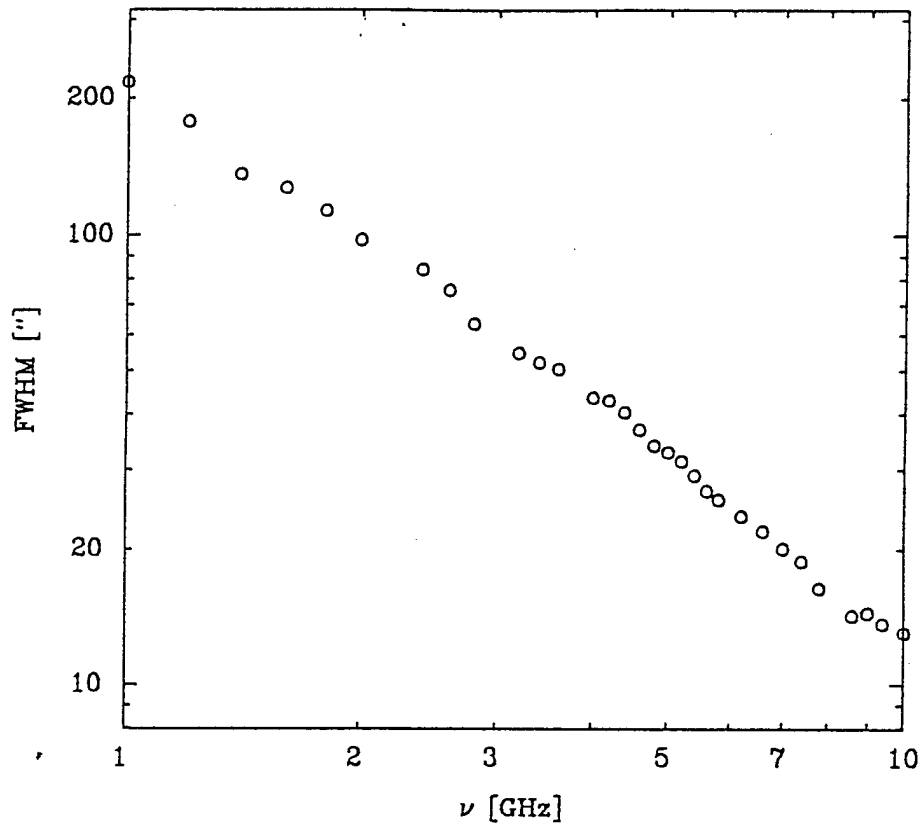
Fig. 2. Full width at half maximum of microwave brightness as a function of observing frequency. Full widths at half maximum are derived from the relative visibility of one baseline at Owens Valley Radio Observatory at the time 20:49 UT on 1990 May 24.

foreshortened. This would not be the case for radio emission if it comes from a high, vertical magnetic loop. Therefore, in order to explain the larger area of radio emission relative to the $H\alpha$ emission, one needs to postulate the presence of a large magnetic loop, which is the main source of the microwave burst.

The observation of total power microwave spectra and its interpretation (Lee, Gary, and Zirin, 1994) also deserves mention. A very distinctive point of the microwave burst during this flare is the huge flux spectrum reaching $\sim 10^4$ solar flare units (s.f.u.) over a wide range of frequencies, 1–18 GHz, at the time of the maximum flux. Lee, Gary, and Zirin (1994) deduced, under the assumption of a nonthermal gyrosynchrotron mechanism, a set of parameters with which the observed flat and high microwave spectra can be reproduced. To get a flux as high as 10^4 s.f.u. even at low frequencies, they require a nonthermal electron

distribution as hard as $N_e(E) \sim E^{-3}$, with $N_e(> 100 \text{ keV}) \approx 3 \times 10^{36}$ and a large physical volume of the source with the height $R \approx 2 \times 10^5$ km and the thickness $2r \approx 6.5 \times 10^4$ km at the apex. To have a flat spectrum, the field strength in the model loop is assumed to vary from 5 G at the loop apex and increasing toward the footpoints according to the dipole field law. The result for the size of the radio brightness and its variation with frequency (Lee, Gary, and Zirin, 1994, their Figure 4) is in a good agreement with the experimental results shown in Figure 2. In the present study, we will examine whether these source parameters derived from a model for microwave observation can be consistent with our results of analysis of the neutron monitor data (see Section 4).

The model results mentioned above are primarily constrained by the observation of total power spectra. This model, however, counts only the contribution from nonthermal electrons and does not estimate the density of thermal particles. To estimate the density of thermal electrons, we may require that the Razin–Tsytovich frequency should be lower than 1 GHz because significant fluxes are seen down to 1 GHz. Thus, from the Razin–Tsytovich frequency, $\nu_{R-Ts} \equiv 2\nu_p^2/(3\nu_{Be}) <$ 1 GHz, we get $n_e < 2.5 \times 10^8$ cm^{-3}. Here, ν_p and ν_{Be} are plasma frequency and electron gyrofrequency, respectively (e.g., Fleishman and Kahler, 1992). Note that the corresponding Alfvén speed is then $V_A > 7 \times 10^7$ cm s^{-1}.

The 1990 May 24 flare is one of the events in which Moreton waves are seen very clearly. The shock wave in this event manifests itself through a fast and bright front of Hα emission that propagates away from the active region as shown in Figure 3. The first three frames (Figure 3(a), 3(b), and 3(c)) show a propagating shock front as marked by the white dotted lines. It is noteworthy that the shock wave is passing through a filament situated perpendicular to the wave front and highly activating the filament as it passes by. The wave front gets faint as it propagates far away from the active region. In Figures 3(d) and 3(e), however, we are able to locate the shock wave front by noticing that another filament (indicated by an arrow in Figures 3(d) and 3(e)) is highly activated by the shock front at a time between 20:49:47 and 20:49:57 UT. The passage of the shock front traced in this way is marked in Figure 3(f) against an Hα picture taken at an earlier time.

To determine the speed and the starting time of the shock, we measure the apparent distances along the east–west direction traversed by the shock (Figure 3(f)) as a function of time and convert them to actual distance along the photospheric surface taking into account the curvature near the limb. The results are shown in Figure 4. If the shock moved out with a uniform speed all the way, then the linear speed would be ≈ 1600 km s^{-1} and the shock must have started at 20:47:40 UT, as indicated in Figure 4. If the original speed was higher and we see it after deceleration to the observed constant speed, the shock could have started later than 20:47:40 UT. It is harder to judge the shock start time by eye because one can recognize shock motion only after the brightening at the shock front is well separated from the source brightening, which is also expanding to an extent. We have examined carefully the Hα movies and found that the shock propagation becomes apparent to
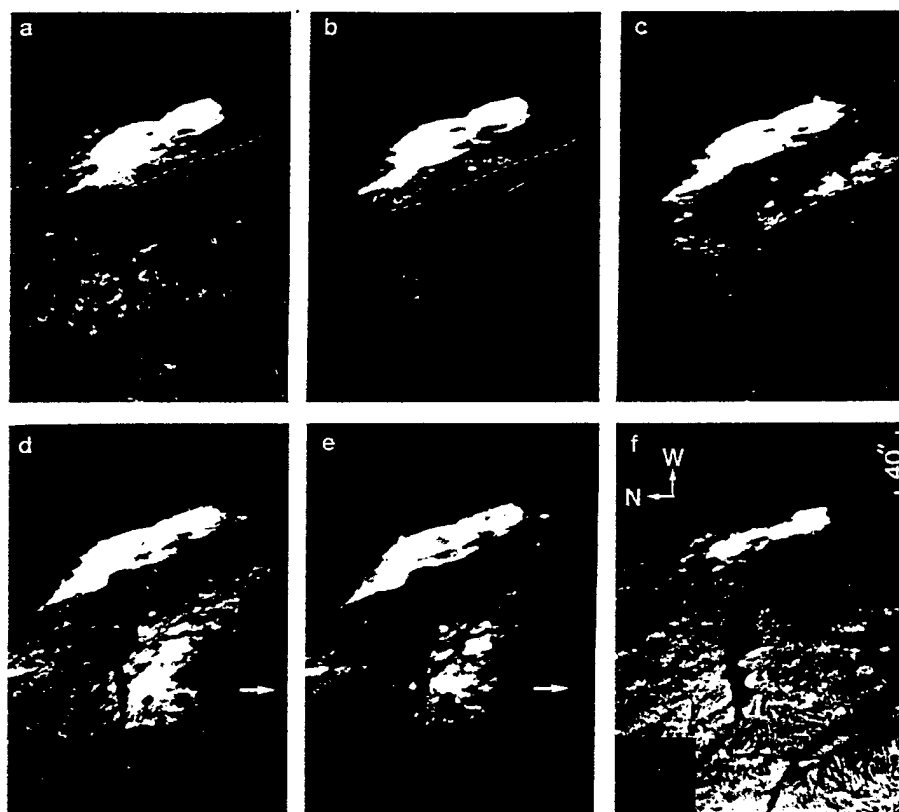
Fig. 3.   Shock-wave propagation: (a)–(c) show the propagating shock-wave front (marked with white dotted lines) as it appeared in the Hα center line. (d) and (e) show the activation of a filament (indicated by arrows) at the arrival of the shock front. (f) summarizes the passage of the shock front.

the eye after 20:47:50 UT. This would set an upper limit for the possible shock start time. Therefore, we presume that the shock had started between 20:47:40 and 20:47:50 UT.

As a result, it appears that the shock preceded the time of maximum microwave radiation by 20–30 s (cf. Lee, Gary, and Zirin, 1994) and that of γ-rays by 40–50 s (see Figure 5(b)). This result naturally leads to a possibility that the shock wave is responsible for accelerating electrons and protons that emit those electromagnetic radiations during the flare.

3. Neutron Emission

The neutron emission associated with the 1990 May 24 flare was recently discussed by Debrunner, Lockwood, and Ryan (1993). In that paper, a fit to the neutron observations was proposed using a time-extended neutron production described by the intensity-time profile of 79.5–109.5 MeV γ-ray emission and a constant neutron emissivity energy spectrum over the whole event. In our analysis, we will
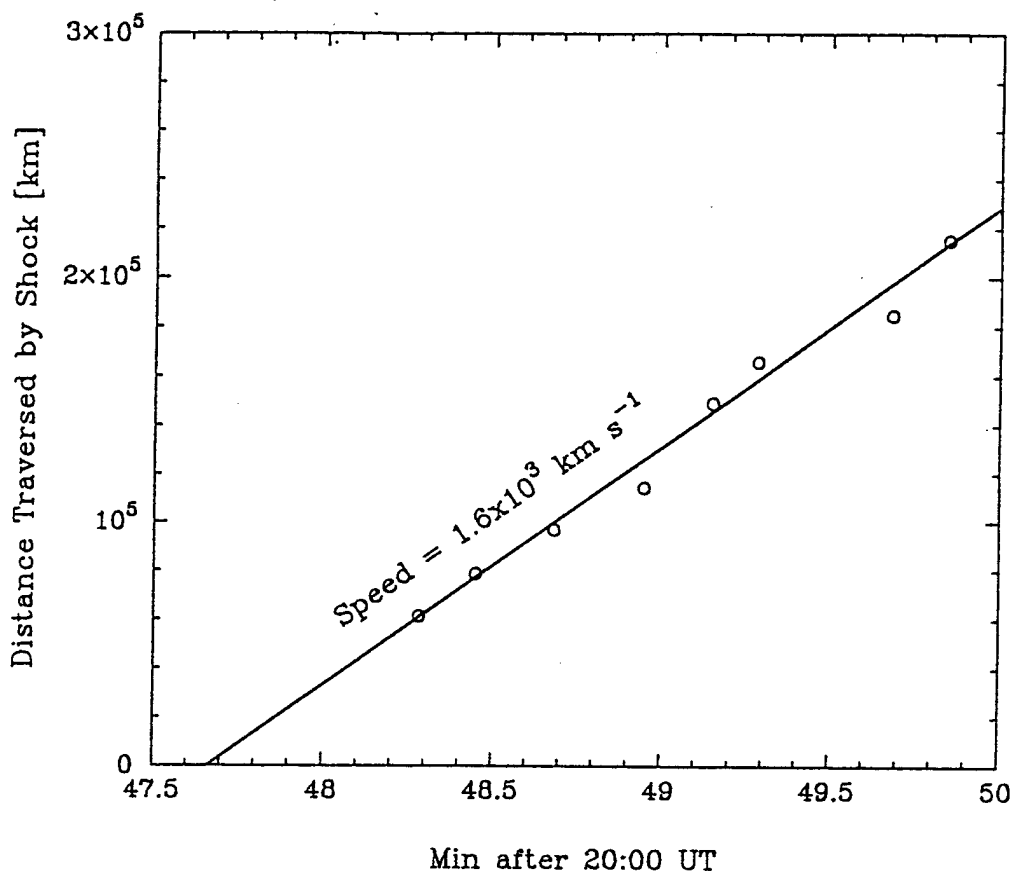
Fig. 4. Linear distance traversed by the shock front as a function of time. Curvature of the surface is corrected for. The speed of the shock is deduced as shown.

look for the best fit to the neutron monitor data by varying four parameters (see below) instead of using the fixed-parameter approach of Debrunner, Lockwood, and Ryan (1993). New information on 2.2 MeV neutron capture γ-ray emission (Terekhov et al., 1993) will also be included. As a result new information will be obtained.

For this event the Climax neutron monitor was at the most favorable location for observation of neutrons from the Sun. We analyse min-by-min data from this neutron monitor in order to study the characteristics of neutron injection from the Sun. Figure 5(a) shows the Climax neutron monitor response for solar neutrons from this flare. The standard deviation is determined by variations of the cosmic-ray background. We took this background as the neutron monitor counting rate averaged between 20:33–20:49 UT. We compared the observed neutron monitor response to solar neutrons with a simulated response for various parameters of neutron injection by means of the χ^2-analysis. We have done it for 14 one-min
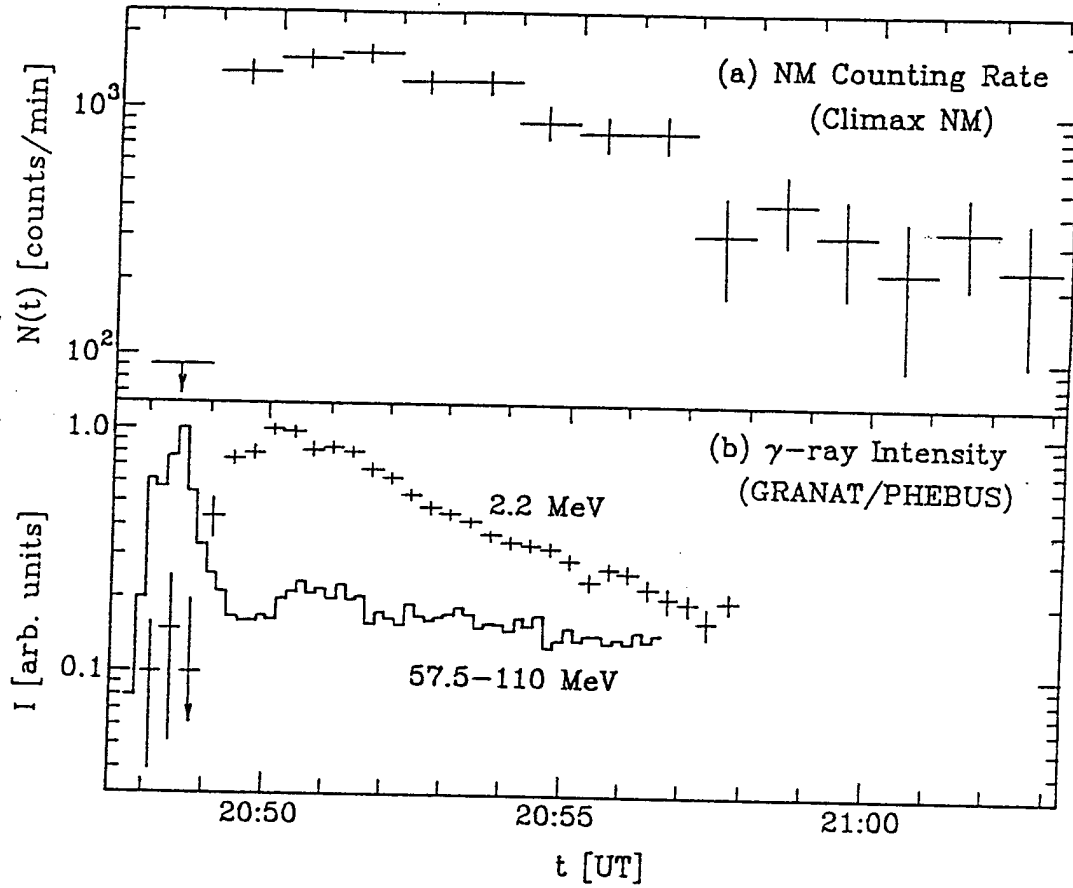
Fig. 5. Time profiles of neutrons and γ-ray emission observed on 1990 May 24: (a) The Climax Neutron Monitor data in 1 min time-intervals; (b) γ-rays at energy 57.5–110 MeV and 2.2 MeV obtained by GRANAT spacecraft (Talon et al., 1993; Terekhov et al., 1993).

intervals from the start of the counting rate increase at 20:49 UT until the moment of the arrival of the first relativistic protons to the Earth's orbit at 21:03 UT . The neutron monitor counting rate, $N(t)$, resulting from a given solar neutron injection at the Sun, $Q(E, t)$, is described as

$$N(t) = \frac{1}{R_a^2} \int\limits_{E_{th}}^{\infty} Q\left(E, t - \frac{R_a}{v}\right) S(E) \exp\left[-\frac{R_a}{\gamma \tau_n v}\right] dE , \qquad (1)$$

where E, v, and γ refer to the energy, the velocity, and the Lorentz-factor of a neutron, respectively; $S(E)$ is the neutron monitor response function for solar neutrons; the exponent describes neutron decay in the interplanetary medium (τ_n is neutron decay time in intrinsic frame of reference); E_{th} is the neutron monitor threshold energy for solar neutrons; $R_a = 1$ AU. The response function $S(E)$

depends on the type of neutron monitor, its altitude and solar zenith angle. We consider the response function of the Climax 12IGY type neutron monitor as that calculated for the Jungfraujoch neutron monitor for the 1982 June 3 flare (Debrunner *et al.*, 1983; Chupp *et al.*, 1987). We make use of this response function because observational conditions (i.e., altitude and solar zenith angle) of both flares were similar. We have taken into account the difference of the effective area of those neutron monitors.

In order to elucidate the possible temporal behavior of neutron injection in this event we used data on the time-profiles of γ-ray intensity from this flare. Such observations were carried out aboard the GRANAT spacecraft (Pelaez *et al.*, 1992; Talon *et al.*, 1993; Terekhov *et al.*, 1993). Neutron monitors are sensitive to solar neutrons >100 MeV. Gamma-ray emission >10 MeV from the π^0-decay carries direct information on the time profile of high-energy neutron generation at the Sun since both the pions and the neutrons are produced by protons of the same energy. Gamma- ray emission >10 MeV could be caused by bremsstrahlung of relativistic electrons as well, but the contribution of this source of γ-ray emission can be determined by means of the spectral shape of γ-rays (Talon *et al.*, 1993). The π^0-decay originated γ-ray emission has a flat spectrum in the 30–100 MeV band while bremsstrahlung-originated γ-ray emission has a steeper spectrum. The time-profile of radiation at 57.5–110 MeV (Talon *et al.*, 1993) is shown in Figure 5(b). One can see a strong pulse of radiation of about 1-min duration. The spectral behaviour of γ-rays during the impulsive phase is rather complicated. Analysis of the temporal behaviour of γ-ray intensity both in the 57.5–79.5 MeV and the 79.5–110 MeV bands (see Figure 10 of Talon *et al.*, 1993) shows that the ratio of these values is >3 before and <2 after 20:48:20 UT. This fact allows one to propose that the π^0-decay originated γ-ray emission at >50 MeV dominated after 20:48:20 UT only. This γ-ray emission peaks at about 20:48:30 UT followed by nearly exponential decay with an *e*-folding decay time of about 20 s (see Figure 5). Note that the increase observed after 20:50 UT is due to the arrival of neutrons (Terekhov *et al.*,1993), so there is no clear evidence that π^0-originated γ-ray emission took place after the impulsive phase. The suggestion that at least half of the total counting rate at 57.5–110 MeV after the impulsive phase was due to neutrons arriving leads us to conclude that the fluence of π^0-decay γ-rays was, at most, not higher in the post-impulsive phase than in the impulsive one.

The temporal behaviour of the neutron capture line at 2.2 MeV also carries information on neutron generation at the Sun. Note that the 'effective' energy of those neutrons (<100 MeV) is too low for detection by the neutron monitor. The 2.2 MeV emission is shown in Figure 5. It peaks at about 20:50 UT, followed by a nearly exponential decay with decay time $T = 180$–360 s (Terekhov *et al.*, 1993); the best fit corresponds to $T \approx 260$ s. Calculations of deceleration, decay and capture of neutrons in the standard solar atmosphere show that in the case of impulsive injection of neutrons into the solar atmosphere, the 2.2 MeV intensity-time profile has the maximum delayed by ~ 3 s and is followed by exponential

decay with an e-folding time $T_d = 70$ s (Wang and Ramaty, 1974). This has been proved by means of observations of the temporal behaviour of the 2.2 MeV line for a number of flares (Prince et al., 1983; Trottet et al., 1993). Thus, the observed decay time of the 2.2 MeV line, $T \gg T_d$, was not caused by the deceleration, decay and capture of the neutrons in the solar atmosphere. This decay time reflects the decay of neutron generation during the post-impulsive phase. Note that in the case of the exponential fall of neutron generation for $T > T_d$ the maximum of the 2.2 MeV line intensity must be delayed by $t_m = T_d a \ln[a]/(a-1)$, where $a \equiv T/T_d$. At $T = 180-360$ s and $T_d = 70$ s the delay time is $t_m = 108-142$ s. This t_m value is close to the observed delay of the 2.2 MeV line maximum with respect to the maximum of γ-radiation at 57.5–110 MeV (see Figure 5). Thus, taking into account available data we propose that the neutron injection time profile is a superposition of two components: the fast injection component has an e-folding decay time of about 20 s and the slow one, of about 200 s. Obviously the contribution of the fast injection component to the neutron generation would be small enough to be in accordance with the 2.2 MeV time profile, but the fast component would give the main contribution to the π^0-generation. Since the pion-to-neutron generation ratio increases with the energy of the primary particles, one can expect that the energy spectrum of the fast injection component would be harder than that for the slow component. It will be shown below that such is indeed the case.

For these reasons, in order to simulate the counting rate of the Climax neutron monitor during this flare we propose the following expression for neutron injection from the Sun:

$$Q(E,t) = N_f \exp[-E/E_f - t/T_f] + N_s \exp[-E/E_s - t/T_s], \qquad (2)$$

where $N_{f(s)}$, $E_{f(s)}$, and $T_{f(s)}$ denote number, energy spectrum, and decay time of the fast (slow) injection component, respectively. Calculations (Hua and Lingenfelter, 1987) show that neutron generation spectra become steeper with energy in a band from tens of MeV up to ~ 1 GeV even if the primary proton spectra follow power laws. The common approximation (power-law neutron spectrum with energy cut-off) is not adequate because it is not sufficiently steep and it requires the cut-off energy as one more parameter. For this reason, we use an exponent over energy for the neutron spectrum as the better approximation. Below we use as a parameter the ratio of the whole number of >100 MeV neutrons in the fast component to that in the slow one,

$$x \equiv \frac{N_f(E > 100\,\text{MeV})}{N_s(E > 100\,\text{MeV})} = y \exp\left[\frac{100\,\text{MeV}}{E_s}\left(1 - \frac{E_s}{E_f}\right)\right], \qquad (3)$$

where $y = N_f T_f E_f/(N_s T_s E_s)$.

In Figure 6 we present 90% confidence contours for the exponential energy constants E_f and E_s. Moreover we make use of an additional limit that the simulated neutron monitor counting rate during the interval 20:48-20:49 UT does not

TABLE I

Best-fit parameters of neutron injection spectra

	x	E_f MeV	N_f (30 MeV) sr^{-1} MeV^{-1}	E_s MeV	N_s (30 MeV) sr^{-1} MeV^{-1}	χ^2 (13)
$T_s = 180$ s	0.1	300	3.8×10^{26}	50	7.3×10^{28}	14.1
	0.2	310	3.5×10^{26}	75	1.5×10^{28}	12.4
	0.3	330	3.0×10^{26}	110	4.3×10^{27}	17.0
$T_s = 220$ s	0.1	300	3.9×10^{26}	50	7.3×10^{28}	15.1
	0.2	320	3.2×10^{26}	80	1.2×10^{28}	10.2
	0.3	340	2.5×10^{26}	130	3.1×10^{27}	11.5
$T_s = 260$ s	0.1	290	4.2×10^{26}	50	7.7×10^{28}	16.7
	0.2	310	3.4×10^{26}	80	1.3×10^{28}	9.6
	0.3	350	2.2×10^{26}	150	2.2×10^{27}	8.9
$T_s = 300$ s	0.1	300	3.9×10^{26}	50	7.1×10^{28}	17.8
	0.2	310	3.5×10^{26}	80	1.3×10^{28}	10.3
	0.3	360	1.9×10^{26}	170	1.7×10^{27}	8.2

exceed the value of 1.3σ which corresponds to the 90% confidence level. The corresponding region is below the dash-dotted line in Figure 6. Another limit is connected with the absence of strong π^0-decay γ-rays after 20:50 UT (Talon *et al.*, 1993; Terekhov *et al.*, 1993). As the generation of π^0-decay γ-rays correlates well with the >500 MeV neutron generation, we require that the number of those neutrons in the slow component be less than their number in the fast one (the corresponding region is situated to the left of the dashed line in Figure 6). Solid circles in this figure correspond to best fits. In Table I we present values for the best fit parameters, E_s, E_f, x, T_s, the corresponding χ^2 values, and numbers of 30 MeV neutrons N_f (30 MeV) and N_s (30 MeV) in the fast and slow injection components, respectively.

In our case of two-component prolonged exponential neutron injection, the time of maximum 2.2 MeV emission may be estimated as

$$t_m = T_d \left(\frac{a}{a-1} \right) \ln[a - (1 - ay + y)] , \tag{4}$$

where $a \equiv T_s/T_d > 1$. In this estimation, we have assumed $T_f \ll T_d$, which may lead to an underestimation of t_m to some extent. From expression (4) it can be seen that at a high value of the fast-to-slow component ratio, $y > a^{-1}$, the 2.2 MeV emission cannot be delayed more than a minute, while the 1990 May 24 maximum of 2.2 MeV emission was shifted in time relative to the maximum of 57.5–110 MeV emission by $\sim$ 90 s (see Figure 5). What is more important, at $y > 0.1$ the fast component neutrons would generate a strong burst of 2.2 MeV
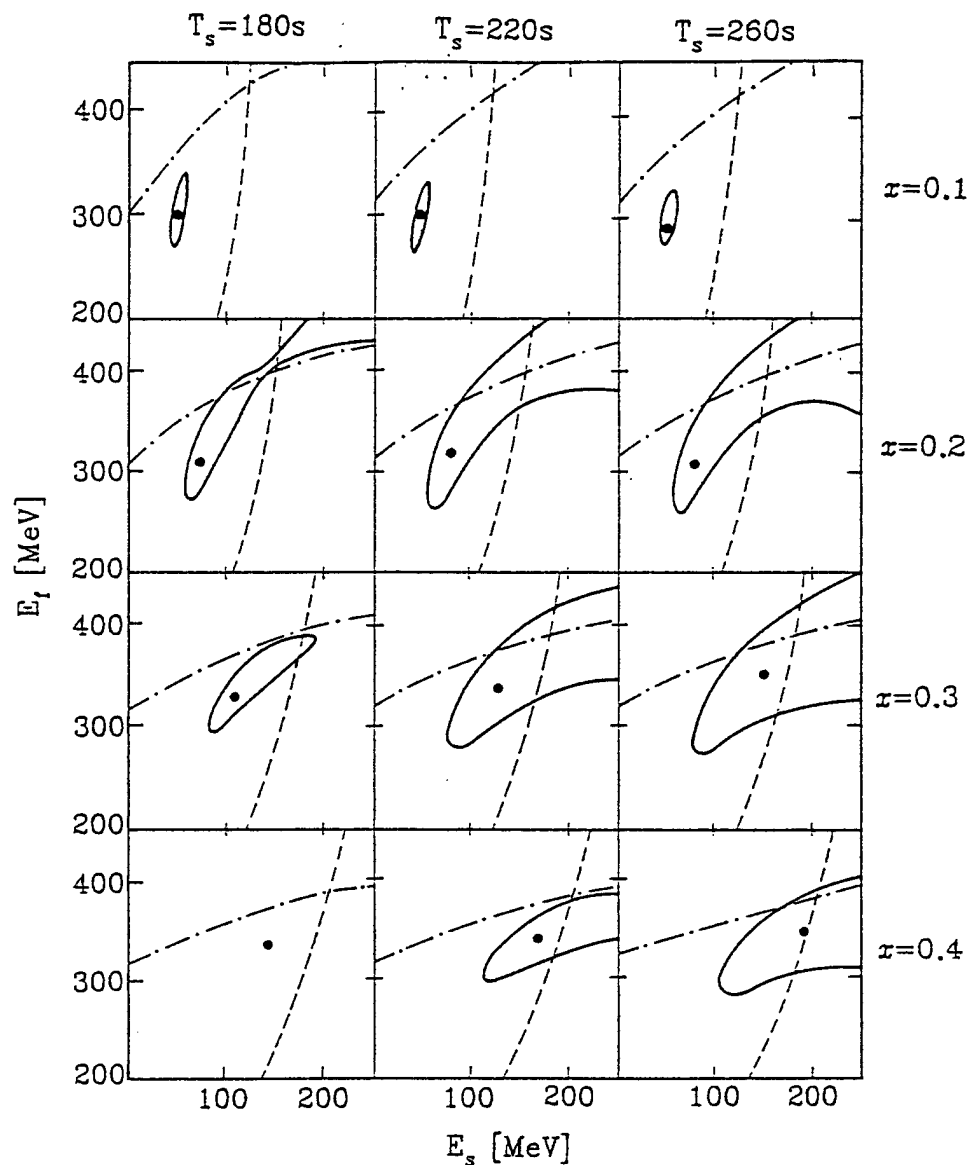
Fig. 6. Results of parameter fitting of Climax neutron monitor counting rate. Each contour represents the 90% confidence level in the (E_f, E_s) plane, for given values of the decay time of the slow component of neutron emission, T_s, and the fast-to-slow components ratio, x. The solid circles in each frame represent the best fit-parameter points. Additional restrictions are denoted by dash-dotted and dashed lines (see text).

emission at 20:48:30–20:49:00 U.T, contradicting the observations. That is why we have to abandon $x > 0.25$.

Thus we obtain the most likely values of the parameters: the decay time of the slow component $T_s \approx 260$ s; the ratio of the whole number of >100 MeV neutrons in the fast component to that in the slow one, $x \approx 0.2$; the characteristic energy of the fast component $E_f \approx 310$ MeV and the characteristic energy of the slow component $E_s \approx 80$ MeV. Note that these results have only a weak dependence on the precise value of T_f because it is less than $T_d = 70$ s (in our calculations $T_f = 20$ s). Using the above parameters the total number of slow component neutrons with energy 30 MeV escaping the Sun in the direction of Earth is $N_n(30 \text{ MeV}) \approx 10^{28}$ MeV^{-1} sr^{-1} and the maximum 2.2 MeV emission delay time is $t_m \approx 100$ s.

Taking into account all uncertainties, we conclude that the total number of >100 MeV neutrons injected from the Sun toward the Earth was not more than 1.1×10^{30} sr^{-1}. One can compare this value with that for the 1982 June 3 neutron event: $\approx 8 \times 10^{28}$ sr^{-1} (Chupp et al., 1987). It is necessary to note that Debrunner, Lockwood, and Ryan (1993) estimated the total number of escaped neutrons on May 24 to be $\approx 5.6 \times 10^{30}$ sr^{-1}. On the contrary, we conclude that on 1990 May 24 the number of escaped 300 MeV neutrons exceeded the number for the 1982 June 3 solar flare by a factor ≈ 7 only (see also Figure 2 of Kovaltsov, Efimov, and Kocharov, 1993). Finally, the harder spectrum of the fast component of secondary neutron emission requires that the spectrum of the primary protons producing this emission be harder too.

4. Implication for Propagation and Interaction of Particles on the Sun

According to the microwave observations presented in Section 2 and the hard X-ray data by Pelaez et al. (1992), the 1990 May 24 solar flare had a simple single-pulse structure. For this type of flare it is natural to test the hypothesis that all particles were accelerated during a short time at the beginning of the flare. With this approach, impulsive acceleration would be followed by some propagation and interaction processes. Then we will attempt a trapping model. We briefly review some results of such models in Section 4.1. In Section 4.2, we estimate the theoretical values of the decay time of secondary emission using the physical parameters of the flare active region (Section 2) for comparison with the parameters derived from neutron monitor data (Section 3).

4.1. THEORETICAL PREDICTIONS FOR THE DECAY TIME OF SECONDARY EMISSION

The effects of propagation of primary particles in magnetic loops on the secondary radiation were considered in a number of papers (see, e.g., Mandzhavidze and Ramaty, 1992, and references therein). It was shown that the scattering of primary particles by MHD waves in the magnetic loop influences the angular distribution

and the decay rate of secondary emission. One can see from Monte-Carlo simulations (Gueglenko et al., 1990) that in the presence of pitch angle scattering the decay of the secondary generation rate is exponential: $Q(t) \sim \exp[-t/T]$. The characteristic decay time of the emission, T, is a function of the MHD turbulent energy level. The approximate expression for the decay time can be found in the case of strong or moderate pitch angle diffusion when the angular distribution of primary particles in the coronal part of the loop can be treated as nearly isotropic (Gueglenko, Kocharov, and Kovaltsov, 1991). In this case, an approximate expression for the decay time can be given as

$$T = \frac{R^2}{D} + \frac{2\pi R}{v(1-\mu^2)} \, , \tag{5}$$

where D is the spatial diffusion coefficient which depends on the turbulence level through the particle mean free path length in the ordinary way; v is the velocity of the particle at some 'effective' energy (it depends on the type of secondaries); μ is the cosine of the loss cone boundary angle. The coronal part of the loop is assumed to be semi-circular, its radius is R. Expression (5) is valid if the mean free path of primary particles, λ is less than $\pi R/(1-\mu)$. Otherwise (i.e., for weak pitch-angle diffusion) the decay time, T, increases with the path length. Thus for a magnetic loop it is impossible to have T less than calculated using the second term in the expression (5). For estimations of the proton free pathlength the following simple expression may be used:

$$\frac{\lambda}{\pi R} \approx \left[\frac{8\pi \mathcal{W}}{(2\times 10^{-5})B^2}\right]^{-1} \left[\frac{n}{10^{10}\,\mathrm{cm}^{-3}}\right]^{-1/4} \left[\frac{\nu_{\min}}{10\,\mathrm{Hz}}\right]^{-1/2} \left[\frac{R}{10^{10}\,\mathrm{cm}}\right]^{-1} , \tag{6}$$

where $\mathcal{W}$ is the energy density of the MHD turbulence and $\nu_{\min}$ is the lower cut-off frequency of the turbulence spectrum. B and n are, respectively, the magnetic field strength and the plasma number density in the corollal part of the loop. Here it was assumed that the power law index of the spectrum of MHD turbulence is equal to 1.5 and the proton energy is 150 MeV ('effective' energy for generation of $\sim$ 50 MeV neutrons). Note that λ should vary as the $\frac{1}{2}$ power of the particle momentum.

It is necessary to note that in the case of high density of accelerated protons the turbulence energy is not arbitrary but would be determined in a self-consistent way, because of the cyclotron instability of the energetic proton distribution (e.g., Bespalov, Zaitsev, and Stepanov, 1986). As a result of this instability, accelerated protons with velocity v and number density n_p amplify the resonant waves with frequency $\nu = (V_A/v)\nu_{Bi}$; where ν_{Bi} is the proton gyro-frequency. The amplification rate is $\Gamma = 2\pi n_p \nu_{Bi}^2/(n\rho v)$, where n is the background plasma density and $\rho = B_2/B_1$ is the mirror ratio. To develop the instability it is necessary to have an amplification rate greater than the attenuation rate of these waves. The attenuation due to collisional dissipation of Alfvén waves is $\delta = (m_e/m_p)\nu_e$, where ν_e is

the electron collision frequency. Note that in the case of low-density plasma the attenuation due to the escape of waves from the loop may be essential too. In the case of instability, the decay time of secondary emission can be found as

$$T = \frac{\pi R}{2kV_{\mathrm{A}}} ,$$

(7)

where the dimensionless coefficient k is in the order of unity and depends on the details of the theoretical model (Gueglenko et al., 1990; Bespalov, Zaitsev, and Stepanov, 1991).

Finally it is necessary to note that the above expressions may also be used for some open magnetic configurations with a magnetic field minimum at some height and (or) with MHD turbulence inside (e.g., for 'helmet' type magnetic configurations). However for simplicity we discuss magnetic loops only.

4.2. APPLICATION TO THE 1990 MAY 24 FLARE

We first consider the observed decay time of the slow injection neutron component and 2.2 MeV γ-ray emissions. In the case of strong pitch-angle scattering on external turbulence using Equation (5) we obtain $\lambda \approx 4 \times 10^8$ cm at $T \approx 260$ s, $\rho \approx 10$, and $R = 2 \times 10^{10}$ cm. From Equation (6), we then have $\mathcal{W}/(B^2/8\pi) \approx 5 \times 10^{-3}(\nu_{\min}/10 \text{ Hz})^{-1/2}$. The fast injection population of primary protons had a harder energy spectrum (see Section 3). According to standard models of the acceleration process, the harder spectrum of accelerated particles may originate either from the higher level of turbulence accelerating and/or scattering the particles, or from the larger size of the acceleration region (see, e.g., Equation (17.33) in the textbook by Toptyghin, 1983; see also Equation (9) in below). However, in the latter case (i.e. at $R > 2 \times 10^{10}$ cm) it is impossible to obtain the observed small decay time, $T_f = 20$ s (see Equation (5) and following discussion). Thus we can propose that the turbulence energy level at the fast component site is higher than at the site of the slow injection component (both during the acceleration and during the decay phase). In this case the decay time of the fast component of secondary neutron emission may be explained by the smaller radius of the loop where primary protons were trapped. For example, proposing $\lambda \approx 10^7$ cm we obtain the fast component loop radius, $R \approx 10^9$ cm. Thus the existence of two loops containing accelerated protons with different energy spectra arises in a natural way from the existence of two components in the high-energy secondary emission observed on 1990 May 24. Note that more complicated 'multiloop' models may be considered too, but we have no need to do it now.

It was mentioned above that neutrons generated in the solar atmosphere may be decelerated and captured at the Sun or they may escape from the Sun and find their way to the Earth. In the first case neutrons generate the 2.2 MeV γ-ray line which may be detected by the GRANAT observatory. In the second case high-energy neutrons produce an increase in the neutron monitor counting rate. The

relative number of escaped and decelerated neutrons depends on the mode of their propagation in the solar magnetic loops. One can estimate the total number of neutrons necessary to produce the 2.2 MeV γ-radiation observed on 1990 May 24. For this purpose, we use results reported by Hua and Lingenfelter (1987) for the case of isotropic distribution of primary particles moving towards the Sun and our own calculations using a thick-target isotropic model of neutron generation. From both sets of calculations the same result can be obtained: for a certain flux of 2.2 MeV radiation and for different power-law spectral indices of primary protons nearly the same number of 30 MeV neutrons are produced in the solar atmosphere, i.e., 2.2 MeV line production and the total 30 MeV neutron production are well correlated. The 2.2 MeV line fluence $F(2.2\,\mathrm{MeV}) = 345 \pm 6\,\mathrm{cm}^{-2}$ was detected on 1990 May 24 (Terekhov $et\ al.$, 1993). Note that according to Section 3 almost all of this fluence was produced by slow-component neutrons. Then the corresponding total number of 30 MeV neutrons of the slow component generated at the Sun on 1990 May 24 can be found. Taking a unit solid angle we obtain: $I_n(30\,\mathrm{MeV}) = 3 \times 10^{28}\,\mathrm{MeV}^{-1}\,\mathrm{sr}^{-1}$ (for helium-3-to-hydrogen ratio in the solar matter 2×10^{-5}). It is seen that the number of decelerated neutrons exceeds the best-fit number of the escaped neutrons (see Table I) by a factor ≈ 3. Comparing this factor with the results of model calculations (Gueglenko, Kocharov, and Kovaltsov, 1991), one can see that the 'attenuation' factor ≈ 3 can be easily explained on the base of the model of secondary generation by protons moving in the magnetic loop in the strong (or moderate) pitch angle diffusion regime (due to the emission of particles propagating towards the Sun). However, the uncertainties are too large to exclude weak pitch angle diffusion, which is still possible if $E_s = 50$ MeV. Note that to produce the above-mentioned number of neutrons it is necessary to have the total number of primary protons $N_p(> 100\,\mathrm{MeV}) \approx 2 \times 10^{32}$.

According to the above discussion of microwave radiation (Section 2) a flat microwave spectrum observed on 1990 May 24 may occur in the case of a large magnetic loop with small plasma density inside. It is important that for the high number of accelerated protons trapped in the loop with volume $\approx 10^{30}$ cm^3 at the moderate mirror ratio, $\rho \leq 10$, the cyclotron instability (Section 4.1) cannot be suppressed by collision, because the plasma density in the large loop is low (see Section 2). In the case of self-generated turbulence, the decay time of neutron emission can be estimated using Equation (7). For $V_A > 7 \times 10^7$ cm s^{-1} (see Section 2) the decay time of neutron emission $T < 450$ s can be obtained. On the other hand, if we propose that the total energy of accelerated particles (≥ 100 keV electrons) does not exceed the thermal plasma density the lower limit for the plasma density can be obtained: $n \geq 10^8 (2 \times 10^7\,\mathrm{K}/T_p)$ cm^{-3}, where T_p is the temperature of the plasma in the loop. Hence $V_A \leq 10^8 (T_p/2 \times 10^7\,\mathrm{K})^{0.5}$ cm s^{-1} and the decay time $T \geq 300(2 \times 10^7\,\mathrm{K}/T_p)^{0.5}$ s. Remember that $T \approx 260$ s was found from neutron monitor observations. Taking into account the real uncertainties of the model calculations, the agreement seems to be good enough. On the other hand, at $\rho \approx 100$ trapping in the presence of external turbulence can explain the

observations too. In any case, we conclude that both the microwave radiation and the slow component of neutron emission can be explained by the proposition that both accelerated electrons and protons were trapped in a large magnetic loop with $R \approx 2 \times 10^{10}$ cm, $B \approx 5$ G, and $n \approx 10^8$ cm^{-3}. Simultaneously the smaller loop would exist to store the fast injection component of accelerated protons. Recall that the small loop was observed in Hα emission before and after the maximum of the flare.

It is interesting to note that conditions in the large loop correspond to the near equipartition of energy between the magnetic field, accelerated particles and thermal plasma with energy density at the level ~ 1 erg cm^{-3} (during the decay phase of the burst the turbulent energy density is proposed to be much less). Zaitsev and Stepanov (1985) proposed that after the impulsive energy release the flute instability of a magnetic loop may lead to the fast eruption of hot plasma and energetic particles out of the flaring loop. The flute instability criterion depends on the plasma parameter $\beta = 8\pi p/B^2$, where p is the pressure of hot plasma and energetic particles and B is the magnetic field in the loop. If $\beta > \beta^* \approx 0.3$–$1.0$, then the fast eruption takes place. Note that in the case of the large loop considered above $\beta \approx \beta^*$. Hence we can propose that the large magnetic loop assumed to explain the microwave data and the slow injection component of neutrons is the last (borderline) loop surviving after the impulsive energy release.

5. Discussion

In this section, we briefly discuss the problem of acceleration of primary particles during the 1990 May 24 solar flare and the implication of our results for several previous studies.

The stochastic acceleration of protons in magnetic loops was considered by Ryan and Lee (1991) and Kovaltsov and Kocharov (1991). The impulsive (nonstationary) stochastic acceleration by an ensemble of shocks in the 'core' of the flare was found to be suitable to explain the observed spectra of accelerated protons generating secondary emission in some flares (Kocharov and Kovaltsov, 1991). On the other hand, in the beginning of the 1990 May 24 flare a Moreton wave was observed, which may be considered evidence for the presence of the shock wave at a very early stage of the flare. For this reason it is natural to consider the shock wave as the possible source of all accelerated particles.

The acceleration of solar particles by the shock wave in the presence of small-scale turbulence was considered in a number of papers (see Lee and Ryan, 1986; Toptyghin, 1983, and references therein). According to Toptyghin (1983, his Equation (18.78)) the time needed to obtain the stationary particle spectrum up to momentum, p, at the shock is found as

$$t = \frac{3D_1^{1/2}(D_1^{1/2} + D_2^{1/2})}{U_1(U_2 - U_1)} \ln \frac{p}{p_0} , \tag{8}$$

where U is the hydrodynamic velocity; D is the diffusion coefficient of particles due to small-scale turbulence; p_0 is the initial (injection) momentum of particles. Here indexes 1 and 2 denote quantities in front of and behind the shock, respectively. Let us set the time, t, equal to the time it takes for the shock to pass the loop, R/U, and express D in terms of particle escape time from the loop (at the moment of the passage of the shock wave): $T_0 = R^2/D$. We then obtain an expression for the maximum momentum, p_m, in the particle spectrum as

$$\ln \frac{p_m}{p_0} = \frac{UT_0}{6R} .$$

(9)

Using the parameters of the loops necessary for the trapping of the particles, we can estimate the right-hand side of the above equation as $0.2(U/V_A)(T_0/T)$, both for the small and the large loops, where T is the escape time at the decay of the burst obtained from the observations. Keeping in mind that the short-scale turbulence energy level necessary during the decay phase is small $(W/(B^2/8\pi) \ll 1)$, it is not improbable to propose the higher turbulence level at the passage of the shock wave to obtain $(U/V_A)(T_0/T) \gg 1$. In this way it is possible to have $\ln[p_m/p_0] \approx 6$, which is sufficient for the acceleration. Note that the theory of diffuse shock acceleration predicts the flattening of the proton spectrum at nonrelativistic energies up to a power-law spectrum index ≈ 1.5.

On the other hand, according to Pelaez et al. (1992) (see their Figure 16) on 1990 May 24 there was no clear evidence of any excess in the nuclear γ-ray line domain during the most intense part of the event, i.e., it was an 'electron dominated' γ-ray event, in which the 4–7 MeV radiation was mainly produced by electron bremsstrahlung (Rieger and Marschhauser, 1990). Thus for this flare we can obtain the upper limit for 4–7 MeV nuclear line fluence, $F_{nl}(4$–7 MeV), only. In this calculation we took into account the reported efficiency of the detector (0.5) and assumed a constant spectrum during the whole activity (see Figure 15 of Pelaez et al., 1992). In this way and using the 2.2 MeV line fluence reported by Terekhov et al. (1993), one can estimate the 4–7 MeV nuclear lines to 2.2 MeV line ratio for the event: $F_{nl}(4$–7 MeV)$/F(2.2$ MeV)<0.3. This implies that the primary proton spectrum at the Sun was very flat in the 30–150 MeV energy band with a power-law index <1.5 (see Hua and Lingenfelter, 1987). This is in agreement with the proposition of shock acceleration of primary protons in this flare.

Another piece of information to check the above propositions comes from the observed intensity and spectral shape of the γ-ray continuum. It is known that the total number of nonthermal electrons can be estimated from either microwave data or hard X-/γ-ray data. Lee, Gary, and Zirin (1994) proposed, based on the calculation of microwave flux, that the total number of nonthermal electrons would be $N_e(> 100$ keV$) \approx 3 \times 10^{36}$ at the time of maximum flux, under the assumption of the gyrosynchrotron radiation mechanism. Some of these microwave-emitting electrons may also produce the hard X-rays and γ-rays via bremsstrahlung if embedded in ambient plasmas. We estimate the number of γ-ray generating electrons, N_e^γ

from the GRANAT data (Pelaez *et al.*, 1992) to compare it with the result from the study of microwave emission, N_e^μ (Lee, Gary, and Zirin, 1994). From the γ-ray spectrum above >500 keV by Pelaez *et al.* (1992, their Figure 16) and from a recent calculation of electron bremsstrahlung by Ramaty *et al.* (1993) we obtain the total number $N_e^\mu (> 500 \text{ keV}) \approx 5 \times 10^{34}$. We also note that the electron spectral index ≈ 3 assumed in the microwave calculations is in agreement with the observed slope of the γ-ray spectrum. Thus it appears that $N_e^\mu / N_e^\gamma \approx 2$. Many authors have discussed the relative number of electrons needed for production of hard X-rays and microwaves (Petrosian, 1990, and references therein). In the solar flare event on 1990 May 24, the following two scenarios could be relevant. First, the precipitation of the microwave-emitting electrons into the lower atmosphere to emit hard X-rays and γ-rays may be inefficient due to a large mirror ratio and large length of the loop. Second, some portion of the accelerated electrons may escape from the loop before precipitating into the footpoints, in view of the observation of energetic electrons ($E > 2$ MeV) in the interplanetary medium (*Solar Geophysical Data*, 1990). On the other hand, other possibilities are also worthy of consideration (see Petrosian, 1990). However, in any case we can conclude that the hard X-/γ-ray observations aboard GRANAT do not contradict the model proposed above for the 1990 May 24 solar flare.

6. Conclusion

In this paper, we studied the 1990 May 24 flare by examining the macroscopic properties of the flare source region based on the optical observations made at Big Bear Solar Observatory and microwave observations at Owens Valley Radio Observatory. We then analyzed the data of the Climax neutron monitor counting rate and γ-rays from the GRANAT to derive the solar neutron injection as a function of time and energy. In this analysis, we postulated the presence of two components for the neutron injection, each of which has an exponential energy and time dependence. As the result of fitting of the calculated neutron counting rate to the Climax neutron monitor data, we deduce that the combination of the fast injection component with $T_f \approx 20$ s and $E_f \approx 310$ MeV and the slow injection component with $T_s \approx 260$ s and $E_s \approx 80$ MeV explains the γ-ray time profiles at 2.2 MeV and 57.5–110 MeV as well as the neutron monitor counting rates.

We gave a brief, physical interpretation of the parameters of these two components in terms of various models for particle transport in a flaring loop. Identifying the region of the fast component with the small loop as appeared in Hα observation, the short decay time of the fast component ($T_f \approx 20$ s) is attributed to the relatively small size of the loop ($\approx 2 \times 10^9$ cm). Our assumption of a large loop as the source of the slow injection component relies on microwave visibility data and the model for the microwave spectrum. The parameters of the slow injection component derived in this paper provided a cross-check for the assumption under an appropriate model for proton transport. The mean life time of the primary pro-

tons is determined by the self-generated turbulence due to the cyclotron instability, which explains the decay time, $T_s \approx 260$ s.

Recently the 1991 June 15 solar flare was discussed in detail (Kocharov *et al.*, 1994). Now we have analysed the 1990 May 24 flare. In both flares, two components of high-energy secondary emission were found: a harder and less intense emission which may originate from the 'core' of the flare and a softer and more intense emission originating from larger region with scale $\approx 10^{10}$ cm. However, the time behavior of secondary radiation in these flares was different. In the case of the 1991 June 15 flare the continuous acceleration of primary particles after the impulsive phase of the flare was found more probable, while in the 1990 May 24 case acceleration of all particles at the impulsive phase gives the simplest explanation of the observational data. From the relative timing of different radiations and the presence of the Moreton wave at the beginning of the 1990 May 24 solar flare, we propose that all particles were accelerated by the shock wave. At the same time we have no reason to reject stochastic (impulsive or continuous) acceleration (or re-acceleration). However, using the data in hand, the 'shock acceleration plus trapping' scenario is seen to be more natural and as a result more probable. Hence it will be the subject of further, more detailed, theoretical investigation.

Taking into account previous and present analyses of different flares, one can see that in all cases the acceleration of electrons and protons can take place in the 'core' of a flare at the scale $\approx 10^9$ cm. In the case of more powerful flares, additional acceleration on scales $\geq 10^{10}$ cm may take place. The latter produce more intensive secondary emission and greater fluxes of energetic particles at the Earth orbit.

Acknowledgements